Hyperfine interactions and local environment of 57Fe probe atoms in perovskite CaMn7O12

Igor Presniakov, Viyacheslav S. Rusakov, Tatyana V. Gubaidulina, Alexey Sobolev, Alexey Baranov, Gérard Demazeau, O. S. Volkova, V. M. Cherepanov, E. A. Goodilin, A. V. Knot'Ko, et al.

Hyperfine interactions and local environment of ^{57}Fe probe atoms in perovskite $CaMn_7O_{12}$

I. A. Presniakov,[1] V. S. Rusakov,[1] T. V. Gubaidulina,[1] A. V. Sobolev,[1] A. V. Baranov,[1,2] G. Demazeau,[2] O. S. Volkova,[1,3] V. M. Cherepanov,[4] E. A. Goodilin,[1] A. V. Knot'ko,[1] and M. Isobe[5]

[1]*Lomonosov Moscow State University, Leninskie Gory, Moscow 119992, Russia*

[2]*ICMCB, CNRS, University Bordeaux 1, site of ENSCPB, 87 Avenue du Dr A. Schweitzer, 33608 Pessac Cedex, France*

[3]*Institute of Radiotechnics and Electronics, Russian Academy of Sciences, Moscow 125009, Russia*

[4]*Russian Research Centre Kurchatov Institute, Moscow 123182, Russia*

[5]*Institute for Solid State Physics, University of Tokyo, 5-1-5 Kashiwa, Chiba 277-8581, Japan*

(Received 22 January 2007; published 14 December 2007)

Mössbauer spectroscopy has been applied for studying the local environment of ^{57}Fe probe atoms within iron-doped $CaMn_7O_{12}$ manganite with a perovskite-like structure. The ^{57}Fe spectra recorded in the paramagnetic temperature range 90 K$<T<$380 K, where $CaMn_7O_{12}$ has a rhombohedral structure ($R\bar{3}$), were discussed supposing Fe^{3+} probe cations to replace manganese in the octahedral ($Mn^{3+}O_6$) and ($Mn^{4+}O_6$) polyhedra. A very small ($<3\%$) part of Fe^{3+} probe cations characterized by very large quadrupole splitting ($\sim$2 mm/s) suggests that a few amounts of ^{57}Fe probe can be substituted for Mn^{3+} in the (9*e*) positions with approximately a square planar surrounding. In the temperature range 380 K$<T<$450 K, the ^{57}Fe Mössbauer spectra undergo a sharp change which can be due to a formation (at $T_{CO}\sim$380 K) and a gradual growth with temperature of the cubic manganite phase ($Im\bar{3}$). At $T\geq$450 K, the ^{57}Fe spectrum reveals single Fe^{3+} sites in an oxygen symmetric octahedral surrounding. This can be well explained by a fast electron exchange $Mn^{3+}\leftrightarrow Mn^{4+}$, leading to the crystallographic equivalence of all MnO_6 positions. At the temperature range $T<T_{M2}$ (=90 K), an appearance of the distributions of the hyperfine magnetic field values at the ^{57}Fe nucleus up to $\sim$350 kOe (at 77.4 K) was observed. This result is an independent experimental evidence of magnetic ordering in the manganese sublattice.

DOI: 10.1103/PhysRevB.76.214407 PACS number(s): 61.18.Fs, 82.90.+j, 83.80.Ab, 61.66.Fn

INTRODUCTION

Perovskite-like manganites are of considerable interest since they exhibit a great variety of structural and magnetic transitions, dramatic change of electrical conductivity, and magnetoresistance effects. These systems are exemplified by double perovskite-like manganites $AC_3Mn_4O_{12}$, in which large diamagnetic cations *A* (Na^+,Ca^{2+},La^{3+},Ce^{3+}-Yb^{3+}) (Refs. 1–3) are in positions with a dodecahedral oxygen environment, Jahn-Teller transition metal cations *C*(Mn^{3+},Cu^{2+}) have a tetracapped rhombic prism oxygen environment, and heterovalent cations Mn^{3+} and Mn^{4+} are located in an octahedral oxygen environment with a different distortion degree versus their electronic configurations. In this paper, we focus on novel local structural features of one of such compounds: the manganese mixed oxide ($CaMn_3^{3+}$) $\times(Mn_3^{3+}Mn^{4+})O_{12}$ (or $CaMn_7O_{12}$) that shows the complexity of experiencing the electronic process of charge ordering (CO) as a function of temperature.

Neutron diffraction[4,5] shows that, at high temperatures ($T>$440 K), $CaMn_7O_{12}$ has a cubic symmetry (space group $Im\bar{3}$), which is in agreement with the lack of ordering of heterovalent Mn^{3+} and Mn^{4+} cations in octahedral coordination. The manganese cations were suggested to be involved in a fast electron exchange $Mn^{3+}\leftrightarrow Mn^{4+}$, leading to the crystallographic equivalence of all the octahedral positions. Nevertheless, at $T_{CO}\sim$409 K, the cubic manganite undergoes a structural phase transition to the rhombohedral phase (space group $R\bar{3}$), which is associated with the electronic processes of charge ordering (CO) and is accompanied by a sharp decrease in electronic conductivity.[6] This transition was attributed[4] to the emergence of an ordered arrangement of heterovalent Mn^{3+} and Mn^{4+} cations into two types of octahedral polyhedra ($Mn^{3+}O_6$) and ($Mn^{4+}O_6$) with a different degree of distortion versus the electronic configuration of manganese cations. In addition, both phases coexist over the temperature interval 409$<T<$440 K.[4,5]

The structural changes in $CaMn_7O_{12}$ with a further decrease in temperature have been studied using neutron diffraction, x-ray diffraction, and synchrotron radiation (SR).[7–11] In particular, it has been shown that the main changes of the structure are due to the anisotropic thermal expansion of the lattice. The observed change at $T\leq$250 K in SR diffraction patterns, weak reflections (2, 1, ε) and (3, 1, ε), where $\varepsilon=0.07(1)$,[11] is considered as the result of modulation in the electric charge distribution in $CaMn_7O_{12}$, which disappears around $T_C\sim$250 K.[11] However, the physical mechanism responsible for this modulation has never been discussed in the literature.

The magnetic properties of $CaMn_7O_{12}$ have been studied in numerous works.[12–16] The temperature dependences of the magnetization of $CaMn_7O_{12}$ measured under field-cooling (FC) and zero-field-cooling (ZFC) conditions have a bending at $T_{M1}=$50 K and $T_{M2}=$90 K; the FC and ZFC curves almost coincide in the range $T_{M1}<T<T_{M2}$ and diverge at $T<T_{M1}$, as observed, in particular, in spin glasses.[17] The occurrence of phase transitions at T_{M1} and T_{M2} is supported by the measurements of thermodynamic properties.[17] Recently, it was suggested based on muon scattering data[18] that, in the range

$T_{M1} < T < T_{M2}$, the manganite becomes separated into two phases: magnetically ordered and paramagnetic. However, the nature of these phase transitions still remains unclear.

The above data on the crystal and magnetic structures of $CaMn_7O_{12}$ allow us to conclude that many physical properties of this compound must be clarified. Contradictions in the interpretation of available experimental data could be eliminated by invoking spectroscopic methods providing an insight into the local structure of the compounds under consideration. One of such methods appears to be the Mössbauer spectroscopy: due to its record energy resolution, this method provides local information on not only the state of the electronic shell of the resonant atom but also on its local crystallographic environment.

Since Mössbauer nuclei are rather limited in number, Mössbauer probe atoms (^{57}Fe, ^{119}Sn, ^{121}Sb, etc.) introduced into the structure of the compound under consideration are widely used. Up to now, the Mössbauer probe spectroscopy has not been used for studying physico-chemical phenomena in the $CaMn_7O_{12}$ lattice. However, the high efficiency of this technique for studying the local structure and magnetic interactions in perovskite-like oxides has been underlined by different studies of manganites $R_{1-x}A_xMnO_3$ (R=rare-earth element; A=Ca or Sr) doped with ^{57}Fe (Refs. 19–22) and ^{119}Sn (Ref. 23) Mössbauer probes.

In this paper, we report the results of the Mössbauer study of valence state and data of the local environment of ^{57}Fe probe atoms in the $CaMn_7O_{12}$ lattice. We are mainly concerned with the local phenomenon of phase transitions at T_{M2} and T_{CO}. Spectra were measured in a wide temperature range 77–500 K, which encompasses the phase transitions reported elsewhere.

EXPERIMENT

The synthesis of ^{57}Fe-doped $CaMn_7O_{12}$ was carried out by a modified ceramic method.[24] At the first stage, stoichiometric amounts of precursors [Mn_2O_3, $CaCO_3$, and ^{57}Fe metal (the selected doping level corresponding to 0.75 at. % of cations located in the octahedral sublattice, if all ^{57}Fe atoms participate to the manganite lattice, its formula can be described as $CaMn_{6.97}Fe_{0.03}O_{12}$] were successively dissolved in hot aqueous nitric acid (33%) with dropwise added H_2O_2 (30%), which was necessary to completely dissolve Mn_2O_3 due to a redox oxidation. Ashless filters were impregnated with the resulting solution, dried and burnt in air. The resulting oxide powder was reground and annealed in a furnace at 800 °C for 24 h to achieve a nitrate-free oxide product. The latter was ground under a heptane in a Fritsch Pulverizette planetary micro-mill. The precursor powder thus prepared was pressed into pellets (d=15 mm) by applying a force of 5 ton. Then, the pellets were annealed at 850 °C in a pure oxygen flow for 48 h.

XRD data were collected at 298 K using a STOE diffractometer (Cu $K\alpha$ radiation). X-ray diffraction diagram for ^{57}Fe-doped $CaMn_7O_{12}$ sample has been analyzed in the space group $R\bar{3}$. No additional peaks, which could indicate the presence of superstructures or modification of the mentioned symmetry, were observed in any of the examined x-ray diffraction diagrams. The samples were found to be a single phase with its lattice parameters corresponding well at room temperature to the known literature data.

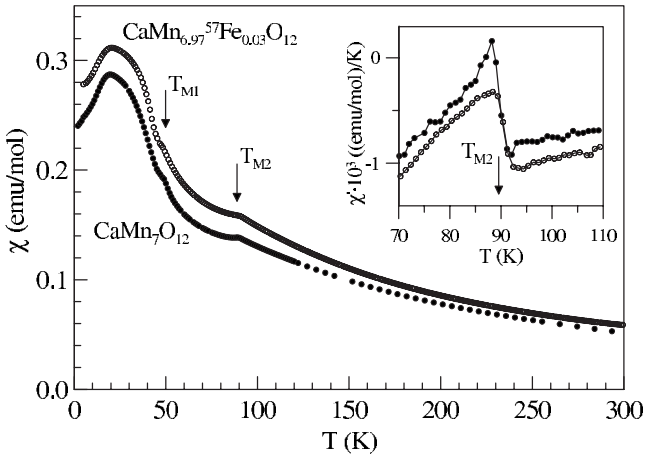

FIG. 1. The plots of magnetic susceptibility χ versus temperature for the samples of double manganites containing (hollow circles) and not containing (filled circles) the probe ^{57}Fe atoms; in the right top corner, the temperature dependences of a derivative value $\chi' = d\chi/dT$ are presented in the vicinity of phase transition at T_{M2}.

DC magnetic susceptibility was measured using a superconducting quantum interference device magnetometer (Quantum Design MPMS) in the temperature range 5–300 K at 10 000 G after zero-field cooling.

The ^{57}Fe Mössbauer spectra were recorded at 77–500 K using a conventional constant-acceleration spectrometer. The radiation source ^{57}Co(Rh) was kept at room temperature. All isomer shifts refer to the α-Fe absorber at 300 K. The experimental spectra were processed and analyzed using the methods of spectral simulation and reconstruction for distribution functions of hyperfine parameters corresponding to the partial spectra implemented in the MS Tools program package.[25] This method has been described in detail in our recent work.[26]

RESULTS AND DISCUSSION

Figure 1 shows the plots of magnetic susceptibility versus temperature $\chi(T)$ for $CaMn_7O_{12}$ and $CaMn_{6.97}Fe_{0.03}O_{12}$. The peculiarities of $\chi(T)$ observed for these polycrystalline samples at T_{M1} and T_{M2} correspond to the low-temperature phase transitions reported earlier. The comparison of these magnetic curves underlines that the stabilization of ^{57}Fe-doped atoms in the $CaMn_7O_{12}$ structure changes neither the thermal dependence of χ nor both low-temperature phase transitions (T_{M1} and T_{M2}) due probably to the low ^{57}Fe doping level. The inset in Fig. 1 shows the derivatives $\chi'(T) = d\chi/dT$ in the temperature range of the second phase transition: evidently, the transition temperature $T_{M2} \approx 90$ K remains almost unaltered within the experimental error.

This finding is strongly different in comparison with the results of earlier Mössbauer studies of ^{57}Fe-doped manganites $R_{1-x}A_xMnO_3$ (R=rare-earth element; A=Ca, Sr),[20,21]

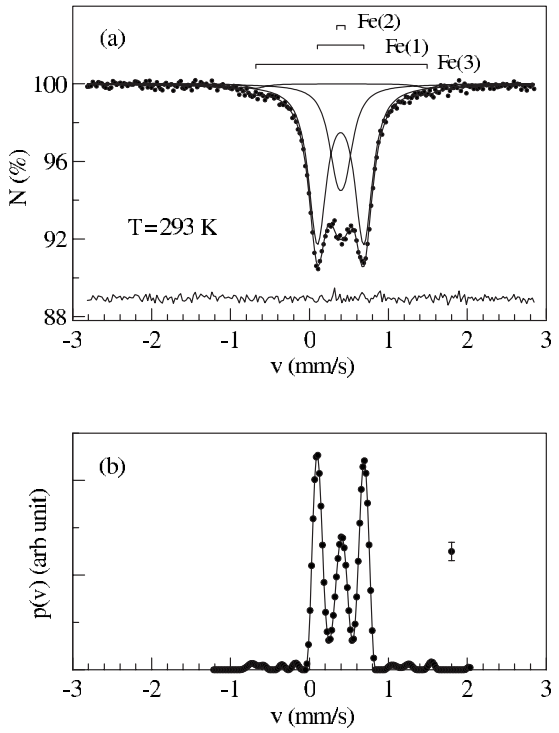

FIG. 2. (a) Modeling reconstruction and (b) distribution functions $p(v)$ of the single resonant line position of Mössbauer spectrum of the $CaMn_{6.97}Fe_{0.03}O_{12}$ sample recorded at $T=293$ K.

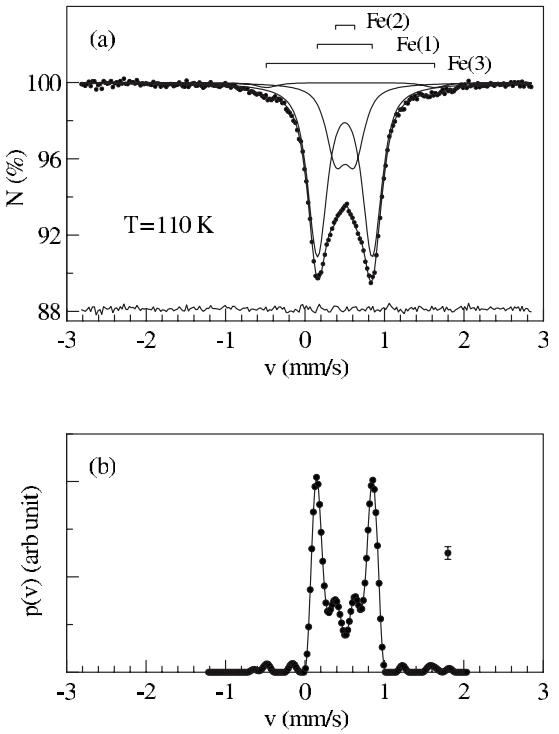

FIG. 3. (a) Modeling reconstruction and (b) distribution functions $p(v)$ of the single resonant line position of Mössbauer spectrum of the $CaMn_{6.97}Fe_{0.03}O_{12}$ sample recorded at $T=110$ K.

which showed that the introduction of a small amount of iron might disturb the electrical and magnetic properties of these oxides. Such a discrepancy would mean (i) that the iron atoms do not enter into the $CaMn_7O_{12}$ structure and form an additional phase difficult to detect by x-ray diffraction due to the small ^{57}Fe doping level or (ii) the physical properties of this $CaMn_7O_{12}$ oxide are completely different than that of the $R_{1-x}A_xMnO_3$ perovskite. The Mössbauer measurements for $CaMn_{6.97}Fe_{0.03}O_{12}$ (see below) showed that the ^{57}Fe spectrum changes considerably in the vicinity of the low-temperature phase transition T_{M2} that confirms a participation of the ^{57}Fe probe atoms to the $CaMn_7O_{12}$ structure. Such a contribution of the ^{57}Fe probe atoms is also confirmed by the drastic changes of the Mössbauer spectrum in the range of the high-temperature structural transition (at $\sim T_{CO}$).

The Mössbauer spectra of $CaMn_{6.97}Fe_{0.03}O_{12}$ measured at temperatures above $T_{M2} \approx 90$ K can be described as a superposition of doublets with different quadrupole splittings. Figures 2(a) and 3(a) show the characteristic spectra observed in the temperature range 110 K $\leq T \leq$ 293 K. At the first stage, in order to enhance the spectral resolution, we reconstructed the distribution functions $p(v)$ of the positions of single resonance lines [Figs. 2(b) and 3(b)].

For the spectrum recorded at $T=293$ K, the $p(v)$ function is a combination of two peaks of approximately equal intensity arranged symmetrically with respect to a third peak with a lower intensity [Fig. 2(b)]. It was shown that in comparison with the $p(v)$ function for the spectrum measured at $T=110$ K [Fig. 3(b)], as the temperature decreases, the distance between the two outer peaks increases, while the central peak is split into two peaks with approximately equal intensity; both the inner and the outer peaks remain symmetrically with respect to the center of the $p(v)$ distribution.

A comparative analysis of the $p(v)$ functions allows to assume that each of the two Mössbauer spectra is a superposition of two main quadrupole doublets with nearly the same isomer shifts δ and significantly different quadrupole splittings Δ. The temperature-induced change in the $p(v)$ functions shows that a decrease in temperature leads to an increase in both the isomer shifts of the doublets and also in their quadrupole splittings.

The model for representing experimental spectra, as a superposition of two major quadrupole doublets attributing to two different irons Fe(1) and Fe(2), is consistent with the results of reconstruction of the distribution functions of isomer shifts $p(\delta)$ and quadrupole splittings $p(\Delta)$ (Fig. 4). The $p(\delta)$ profiles for both spectra are similar to the *Dirac-delta* function, confirming that both quadrupole doublets have nearly the same isomer shifts. At the same time, each of the distribution functions $p(\Delta)$ shows two clear maxima; each of them can be attributed to a definite position of ^{57}Fe atoms into the $CaMn_{6.97}Fe_{0.03}O_{12}$ structure.

In a second step, taking into account the results of the $p(v)$, $p(\delta)$, and $p(\Delta)$ profile analysis, theoretical spectra were simulated to fit the experimental ones [Figs. 2(a) and 3(a)]. This simulation showed that, to adequately describe these spectra, a third quadrupole doublet Fe(3), with a very large quadrupole splitting and insignificant ($\sim 2\%$) partial contribution, should be introduced.

The best-fit hyperfine parameters of the Fe(1), Fe(2), and Fe(3) partial spectra are given in Table I. The isomer shifts of

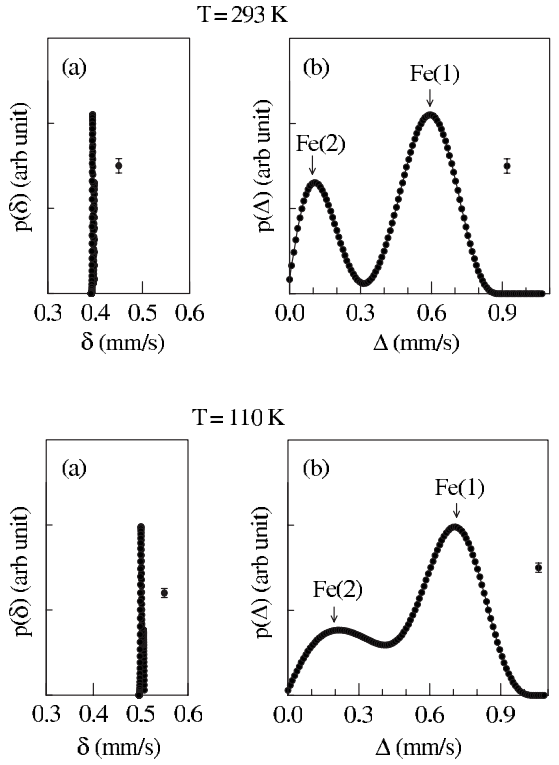

FIG. 4. Distribution functions of (a) the isomer shifts $p(\delta)$ and (b) the quadrupole splittings $p(\Delta)$ of Mössbauer spectra of the $CaMn_{6.97}Fe_{0.03}O_{12}$ sample recorded at $T=293$ and 110 K.

the three quadrupole doublets correspond to high-spin Fe^{3+} ($3d^5$, $S=5/2$) cations in the (FeO_n) sites with high oxygen coordination numbers ($n \geq 6$).[27] However, the noticeably different quadrupole splittings corresponding to the doublets suggest that the Fe^{3+} cations in the $CaMn_{6.97}Fe_{0.03}O_{12}$ manganite structure are distributed over positions with significantly different local symmetries of anionic polyhedra FeO_n.

To interpret the Fe(1), Fe(2), and Fe(3) partial spectra, we should take into account that an ordering of heterovalent cations Mn^{3+} and Mn^{4+} leads to the formation of two types of octahedra in the structure of $CaMn_7O_{12}$: ($Mn^{3+}O_6$) and ($Mn^{4+}O_6$) at ($9d$) and ($3b$) crystallographic positions, respectively, of the rhombohedral structure [Fig. 5(a)]. The Mn^{3+} cations being characterized by a Jahn-Teller electronic configuration ($t_{2g}^3 e_g^1$), the anionic polyhedra ($Mn^{3+}O_6$) are more

TABLE I. Parameters obtained from ^{57}Fe Mössbauer spectra of manganite $CaMn_{6.97}Fe_{0.03}O_{12}$.

T (K)	Subspectrum	δ (mm/s)	Δ (mm/s)	I (%)
293	Fe(1)	0.394±0.001	0.588±0.002	70±1
	Fe(2)	0.399±0.002	0.106±0.010	28±1
	Fe(3)	0.406±0.029	2.170±0.060	2±1
110	Fe(1)	0.500±0.001	0.690±0.002	70±1
	Fe(2)	0.505±0.002	0.240±0.002	28±1
	Fe(3)	0.571±0.019	2.118±0.040	2±1

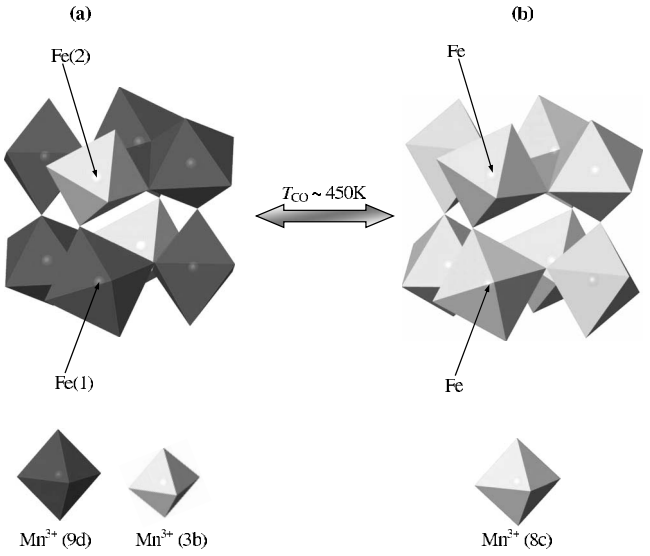

FIG. 5. A polyhedral representation of the crystal structure of $CaMn_{6.97}Fe_{0.03}O_{12}$ (a) above and (b) below the temperature (T_{CO}) of phase transition $R\bar{3} \rightarrow \mathrm{Im}\,\bar{3}$.

distorted than the ($Mn^{4+}O_6$) polyhedra containing an isotropic electronic configuration: Mn^{4+} ($t_{2g}^3 e_g^0$). Taking into account the preference of high-spin Fe^{3+} cations to stabilize in an octahedral oxygen coordination, as well as the proportion between the quadrupole splittings of two major partial spectra ($\Delta_1 \gg \Delta_2$), we should assume that the Fe(1) doublet, with larger quadrupole splitting, arises from the Fe^{3+} cations substituted for the Jahn-Teller cations $Mn^{3+}(3d^4)$ with a distorted octahedral environment. The Fe(2) doublet, with smaller quadrupole splitting, can be assigned to the Fe^{3+} cations substituted for the $Mn^{4+}(3d^3)$ cations with a symmetric oxygen surrounding [Fig. 5(a)].

It is worth noting that the intensity ratio of the partial spectra, $I_1/I_2=2.6-2.8$, somewhat differs from the ratio $[Mn^{3+}]/[Mn^{4+}]=3$ for the population of the octahedral Mn^{3+} and Mn^{4+} positions in nonsubstituted manganite $(CaMn_3^{3+}) \times (Mn_3^{3+}Mn^{4+})O_{12}$. This finding could result that spherically symmetric Fe^{3+} probe cations ($t_{2g}^3 e_g^2$) have a strong preference to substitute for manganese in undistorted ($Mn^{4+}O_6$) polyhedra. This result could be surprising since the ionic radii $r(Mn^{4+})=0.530$ Å and $r(Fe^{3+})=0.645$ Å (Ref. 28) in the octahedral oxygen surroundings are rather different, whereas the ionic radii of Fe^{3+} and Mn^{3+} (0.647 Å) are very close to each other. It is likely that the preferred substitution of the iron cation for a manganese cation (Mn^{3+} or Mn^{4+}) is determined by not only the steric effects but also by the optimization of the electronic configuration of the substituting cation to the symmetry of the corresponding oxygen arrangement in ($Mn^{n+}O_6$) polyhedra inducing the splitting of the $3d$ orbitals.[29] High-spin Fe^{3+} cations are characterized by an isotropic electronic configuration ($t_{2g}^3 e_g^2$); therefore, from the standpoint of the symmetry of (MnO_6) anionic polyhedra, the substitution of Fe^{3+} for $Mn^{4+}(t_{2g}^3 e_g^0)$ cations is favored.

The third quadrupole doublet Fe(3), with almost the same isomer shift as for Fe(1) and Fe(2) and the largest quadrupole

TABLE II. Effective charges (Z) determined from the bond valence model for Ca, Mn, and O within the CaO_{12} and MnO_6 coordination polyhedra in $CaMn_7O_{12}$.

	Octahedral oxygen coordination		"Square" oxygen coordination			
Position	$Mn^{3+}_{(2)}$	$Mn^{4+}_{(3)}$	$Mn^{3+}_{(1)}$	Ca^{2+}	$O^{2-}_{(1)}$	$O^{2-}_{(2)}$
Z	+3.282	+3.915	+3.006	+1.998	−2.073	−2.056

splitting (Table I), corresponds to Fe^{3+} cations stabilized in a very distorted oxygen surrounding. Thus, this partial spectrum can arise either from the Fe^{3+} cations substituted for manganese in $[Mn^{3+}(O_{(1)})_4]$ positions ($9e$), with a nearly square oxygen coordination, or from the iron cations located at the surface of manganite grains. It is worth noting that similar partial spectra with anomalously high quadrupole splitting were observed for other ^{57}Fe-doped perovskite-like manganites.[21,30] Due to the fact that the contribution of the Fe(3) subspectrum is small (~2%), it is difficult to accurately determine its hyperfine parameters; therefore, the behavior of this contribution is not discussed in the following parts.

To independently verify the correctness of the assignment of the partial spectra Fe(1) and Fe(2) to the corresponding positions of the iron cations in the crystal lattice of $CaMn_{6.97}Fe_{0.03}O_{12}$, we calculated a tensor of the electric field gradient (EFG) at Fe^{3+} cations substituted for manganese in the $(Mn^{3+}O_6)$, $(Mn^{4+}O_6)$, and $[Mn^{3+}(O_{(1)})_4]$ positions.

In the general case, the EFG tensor ($\boldsymbol{G}$) at ^{57}Fe nuclei is characterized by two components,[31]

$$\boldsymbol{G} = (1-R)\boldsymbol{G}^{el} + (1-\gamma_\infty)\boldsymbol{G}^{lat}, \tag{1}$$

where $\boldsymbol{G}^{el}$ is the electronic contribution related to the nonuniform distribution of electrons over valence orbitals of the iron cation, and $\boldsymbol{G}^{lat}$ is the lattice contribution induced by the distortion of the crystallographic surrounding of ^{57}Fe nuclei; R and γ_∞ correspond to the Sternheimer shielding ($R>0$) and antishielding [$\gamma_\infty=-9.14$ (Ref. 32)] factors. Due to the spherical symmetry of electron configuration and uniform electron density distribution over all five $3d$ orbitals in the case of high-spin cations $Fe^{3+}(S=5/2)$, it was suggested that it is possible to neglect the electron contribution, taking into account only the lattice contribution for the following EFG calculations.

Calculations of the EFG tensor have been performed within the ionic model using monopole contributions from each t ion, occupying crystallographically nonequivalent positions. Crystallographic parameters used in calculations have been taken from Ref. 33. Components of a tensor were calculated as follows:

$$G_{ij} = \sum_t Z^t \left[\sum_{k(t)} \frac{3x_i^k x_j^k - \delta_{ij}(r^k)^2}{(r^k)^5} \right], \tag{2}$$

where Z^t is the charge of t ion, $k(t)$ is the summarized index on all positions of t ion, x_i^k and r^k are the Descartes coordinates and radius vector of t ion in position $k(t)$, and δ_{ij} is the Kronecker symbol.

The values of effective charges Z^t were calculated within Brown's model,[34] suggesting the correlation between an effective charge of t-type ion and the sum of its "bond's valences" s_i^t in a respective atomic surrounding,

$$Z^t = \sum_i s_i^t = \sum_i \exp[(r_0 - r_i^t)/B], \tag{3}$$

where r_i^t are interatomic distances in polyhedra incorporating the t ions: CaO_{12} and $Mn(i)O_n$; r_0 and B are the constants, which characterize individual Ca-O and Mn(i)-O bonds. The obtained effective charges Z^t are given in Table II.

The EFG tensors, calculated for each ^{57}Fe nuclei occupying corresponding crystallographic positions of Mn^{m+} ions of the $CaMn_7O_{12}$ manganite structure, have been used to estimate the quadrupole splitting values Δ for the Fe(1) and Fe(2) subspectra,

$$\Delta = \frac{e^2qQ}{2}\left(1 - \frac{\eta^2}{3}\right)^{1/2}, \tag{4}$$

where eQ is the nucleus quadrupole moment [for ^{57}Fe $eQ=0.14$ barn (Ref. 31)], $eq \equiv G_{zz}$ is the main component of the EFG tensor, and $\eta \equiv (G_{xx}-G_{yy})/G_{zz}$ is the parameter of asymmetry.

The quadrupole splittings calculated by Eq. (4) $\Delta_1^{(theor)}=0.68$ mm/s and $\Delta_2^{(theor)}=0.13$ mm/s, corresponding to Fe^{3+} cations in $(Mn^{4+}O_6)$ and $(Mn^{3+}O_6)$ polyhedra, respectively, are in good agreement with the experimental values $\Delta_{1,2}^{(exp)}$ (Table I). Thus, we assure that the model used for the interpretation of the experimental spectrum is fully adequate and its subspectra are correctly assigned to the definite positions of Fe^{3+} cations in the $CaMn_{6.97}Fe_{0.03}O_{12}$ crystal lattice. It is worth noting that $\Delta_{1,2}^{(theor)}$ were calculated using the crystallographic data for unsubstituted manganite $CaMn_7O_{12}$. Hence, good agreement between the $\Delta_{1,2}^{(theor)}$ and $\Delta_{1,2}^{(exp)}$ evidences that the dopant Fe^{3+} cations stabilized in the manganite structure not only do not disturb its crystal lattice but also retain the basic features of the symmetry of the Mn^{3+} and Mn^{4+} anionic surrounding after Mn cations are substituted.

Figure 6 shows the $\delta_{1,2}(T)$ and $\Delta_{1,2}(T)$ plots in the temperature range 90–298 K. For both the subspectra, the $\delta_{1,2}$ and $\Delta_{1,2}$ values monotonically increase with decreasing temperature. It points to the absence of changes in the valence state and local crystallographic surrounding of the dopant ^{57}Fe atoms. In particular, the Mössbauer spectra showed no

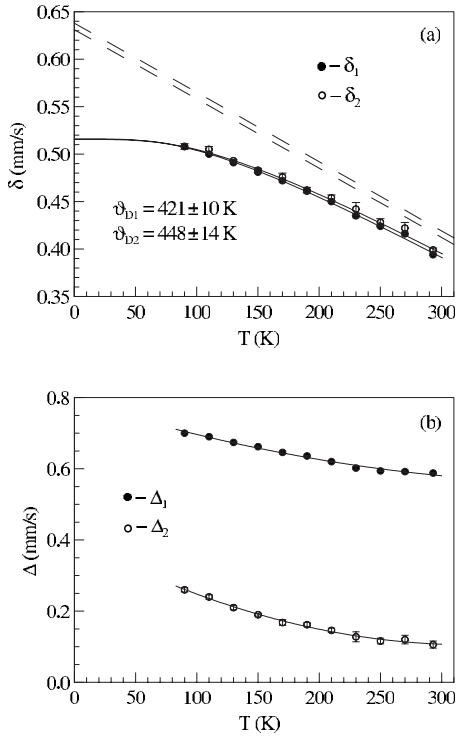

FIG. 6. The plots of (a) the isomer shifts and (b) the quadrupole splittings versus temperature for the subspectra Fe(1) and Fe(2) [high-temperature extrapolation is shown by dashed lines, see Eq. (5)].

structural changes in the crystal lattice of $CaMn_{6.97}Fe_{0.03}O_{12}$ at $T_c=250$ K, which could be attributed to the appearance of the charge modulation.[11]

The experimental $\delta_{1,2}(T)$ and $\Delta_{1,2}(T)$ curves were described using the Debye approximation,[35]

$$\delta(T;\vartheta_D) = \delta^{el} + \delta_T(T;\vartheta_D) = \delta^{el} - \frac{9k_B\vartheta_D}{4mc}\int_0^1 x^3 cth\left(\frac{\vartheta_D}{2T}x\right)dx, \tag{5}$$

where δ^{el} gives the electronic contribution depending on the electron density at ^{57}Fe nucleus, $\delta_T(T:\vartheta_D)$ is the second-order Doppler shift, and ϑ_D represents the effective Debye temperature. Least-squares approximation was performed using a modified linearization method. The best fit for effective Debye temperatures $\vartheta_{D1}=421\pm10$ K and $\vartheta_{D2}=448\pm14$ K are in good agreement with the corresponding values for the dopant Fe^{3+} ions in matrices of other oxide compounds of transition metals.[36,37]

The distance between the dashed lines shown in Fig. 6 corresponds to the difference between the electronic contributions δ^{el} [see Eq. (5)] to the isomer shifts of the Fe(1) and Fe(2) partial spectra. This difference can be associated with the unequal populations (m) of the valence 4s orbitals of the formally trivalent cations Fe^{3+} ($3d^5 4s^m$) (Ref. 27) substituting for the manganese ions in ($Mn^{3+}O_6$) and ($Mn^{4+}O_6$) polyhedra. Inasmuch as the δ^{el} value should decrease with an increase of the ns electron density at the ^{57}Fe nuclei, the

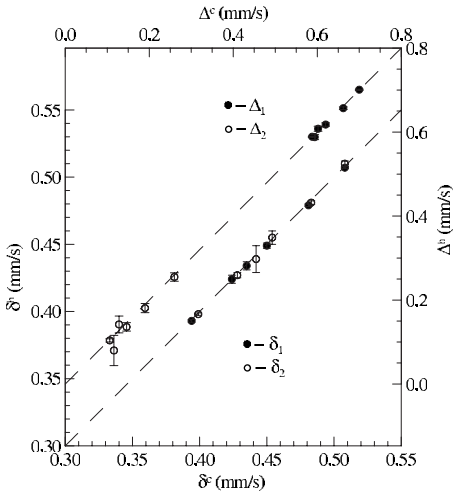

FIG. 7. The correlated changes versus temperature of shifts δ and quadrupole splittings Δ of Mössbauer spectra of the $CaMn_{6.97}Fe_{0.03}O_{12}$ sample recorded in the cooling (δ^c, Δ^c) and heating (δ^h, Δ^h) modes.

observed difference $\delta_2^{el}-\delta_1^{el}=0.007\pm0.003$ mm/s means that the Fe^{3+} cations substituting for Mn^{4+} in small ($Mn^{4+}O_6$) polyhedra acquire a higher positive effective charge as compared to the Fe^{3+} cations in bulky ($Mn^{3+}O_6$) polyhedra. We may assume that the dopant Fe^{3+} cation adjusts its electronic shell to match the size of the surrounding anionic polyhedron, thus compensating for the difference between the ionic radii $r(Fe^{3+})$ and $r(Mn^{4+})$. The additional reason of the distinction between the electronic contributions δ^{el} to the isomer shifts of the Fe(1) and Fe(2) partial spectra can consist that the different geometry of [Fe(1)O_6] and [Fe(2)O_6] polyhedra leads to a different charge distribution in the partially filled $3d^5$ orbitals of the formally Fe^{3+} ions and changes the screening of the filled ns orbitals ($n=1-3$).[27]

In addition, the spectra recorded in the "cooling" and "heating" modes did not show hysteresis in the $\delta_{1,2}(T)$ and $\Delta_{1,2}(T)$ dependences (Fig. 7); such hysteresis was previously observed for perovskite-like manganites $La_{1-x}Ca_xMnO_3$: ^{57}Fe.[21] Actually, according to Fig. 7, the changes versus temperature of shifts δ and quadrupole splittings Δ of Mössbauer spectra for the manganite $CaMn_{6.97}Fe_{0.03}O_{12}$ recorded in the cooling and heating modes are correlated. Also, the proportional changes of corresponding hyperfine parameters versus temperature are observed.

According to Fig. 8, a transformation of manganite $CaMn_{6.97}Fe_{0.03}O_{12}$ to the cubic structure at $T\geq380$ K is accompanied by a sharp change in its Mössbauer spectrum. The profiles of the reconstructed distribution functions $p(v)$ show that, as the temperature increases in the range 380–450 K, the intensity of the central peak gradually increases while the intensities of the two outermost peaks corresponding to the Fe^{3+} cations in the ($Mn^{3+}O_6$) positions of the rhombohedral manganite structure decrease. Above $T\approx450$ K, the experimental spectrum is represented by a single unresolved doublet with parameters close to those of the Fe(2) partial spectrum at $T=300$ K (Fig. 2) [with regard to the temperature-induced shift $\delta_T(T,\vartheta_D)$, see Eq. (4)].

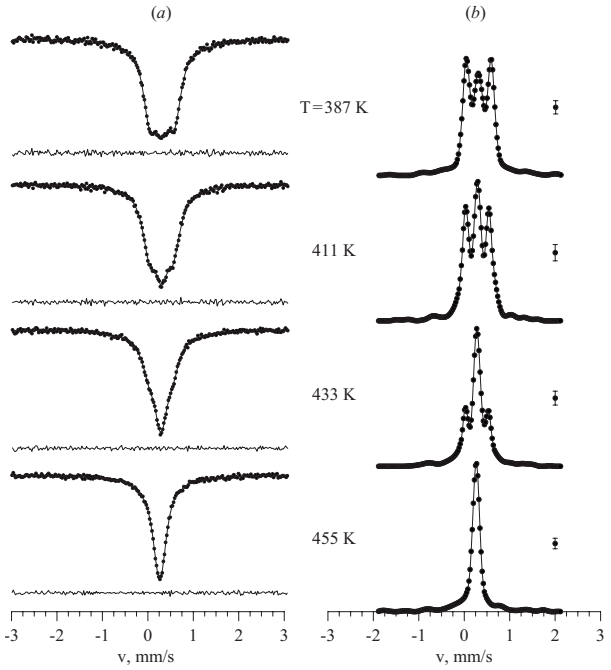

FIG. 8. (a) Mössbauer spectra and (b) corresponding distribution functions $p(v)$ of the single resonant line position in the temperature range $T \geq 293$ K.

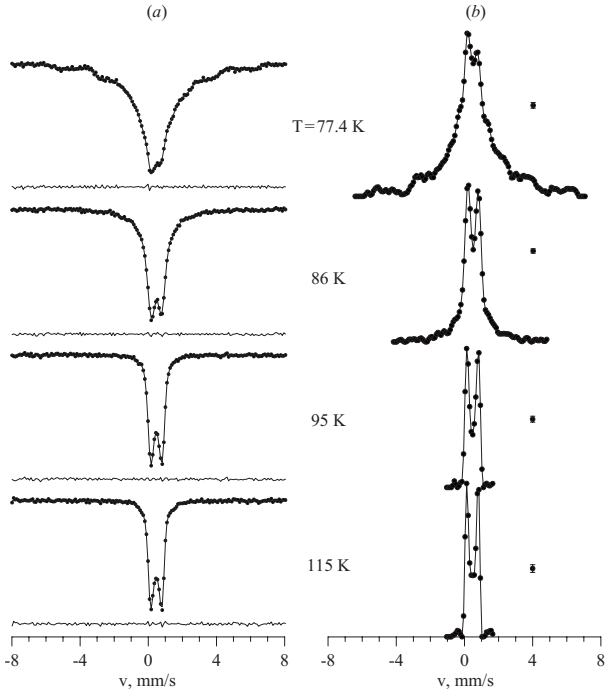

FIG. 9. (a) Mössbauer spectra and (b) corresponding distribution functions $p(H_n)$ of the magnetic field for ^{57}Fe nuclei in the temperature range $T < T_{M2}$.

The above changes in the Mössbauer spectrum of $CaMn_{6.97}Fe_{0.03}O_{12}$ are qualitatively in agreement with the data obtained by high-temperature x-ray diffraction for unsubstituted $CaMn_7O_{12}$,[4,5] which show that the formation of the cubic phase is accompanied by averaging of all manganese octahedra to give only one type of octahedral ($Mn^{3+}O_6$) position close by local symmetry to the Mn^{4+} position in the manganite rhombohedral lattice ($T < T_{CO}$) [Fig. 5(b)]. These data can be taken into account for the presence of the single quadrupole doublet with hyperfine parameters close to those of the Fe(2) partial spectrum of rhombohedral manganite in the high-temperature Mössbauer spectra of $CaMn_{6.97}Fe_{0.03}O_{12}$.

Thus, we have to assume that in the temperature range 380–450 K, the central peak of the $p(v)$ distribution [Fig. 8(b)] corresponds well to two states of iron cations with very close hyperfine parameters: (i) to the Fe^{3+} cations in the (3*b*) positions ($Mn^{4+}O_6$) of the rhombohedral $CaMn_{6.97}Fe_{0.03}O_{12}$ phase [Fig. 5(b)] and (ii) to the Fe^{3+} cations substituting for manganese in the averaged octahedral positions ($Mn^{3.25+}O_6$) being involved in a fast electron exchange $Mn^{3+} \leftrightarrow Mn^{4+}$ [Fig. 5(b)]. The coexistence of the partial spectra corresponding to the rhombohedral and cubic manganite phases in this temperature range is supported by the results of the synchrotron study of $CaMn_7O_{12}$ (Refs. 4, 5, and 38) involving the coexistence of two phases. The high-temperature phase transition $R\bar{3} \rightarrow Im\bar{3}$ is accompanied by the nucleation of the cubic phase; as the temperature increases in the range 400–450 K, these nuclei gradually grow, while the fraction of the rhombohedral manganite phase progressively decreases.

In the low-temperature range $T < T_{M2}$, a noticeable broadening of the resonance lines in the spectra is observed [Fig. 9(a)], which evidences for the existence of a continuous distribution of hyperfine magnetic fields (H) at the ^{57}Fe nuclei. In order to obtain the hyperfine interaction parameters for the temperature range 77–95 K, where the paramagneticlike and magneticlike contributions appear to coexist, the spectra in this temperature range were analyzed using the method of a distribution-function restoration of the static hyperfine fields (H_n).[26] The objective of this analysis was to examine the quality of fitting achievable under the assumption that all the probe iron atoms are in a magnetic state below T_{M2}.

The distribution functions $p(H_n)$ obtained at different temperatures are shown in Fig. 9(b). The $p(H_n)$ profiles for the spectra at 95–90 K range are similar to the Dirac-delta function corresponding to the paramagnetic phase. For the 86–77 K temperature range, there are two regions in the distribution functions; the first of them (low-field peak) corresponds to the paramagnetic or relaxed part of the spectrum and the second diffuse region can be related to the magnetic part of the spectrum. Figure 10 shows the changes versus temperature for a dispersion $D_{p(H_n)} = \overline{(H_n - \bar{H}_n)^2}$ of the distribution function $p(H_n)$ and for an average value of magnetic hyperfine field $\bar{H}_n(T)$. It was observed that a sharp increase of the $D_{p(H_n)}$ value takes places in the vicinity of $T = 90 \pm 2$ K, which practically coincides with the phase transition at the T_{M2} point.[12–16] This result seems to be an independent experimental evidence for the emergence of a magnetic order of manganese cations (Mn^{3+} and Mn^{4+}) at $T < T_{M2}$, which forms the octahedral cationic sublattice of the manganite $CaMn_7O_{12}$.

It is important to note that when the temperature decreases, the low-field peak in the distribution function $p(H_n)$

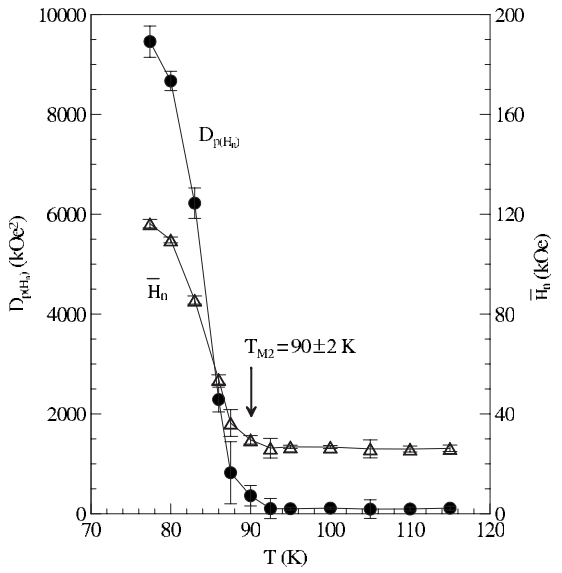

FIG. 10. Temperature dependence of dispersion $D_{p(H_n)}$ of distribution function $p(H_n)$ and an average value $(\bar{H}_n)$ of the magnetic field for ^{57}Fe nuclei.

progressively diminishes, although its position remains nearly temperature independent. This behavior suggests that the apparent low-field contribution should actually be paramagnetic in nature with some quadrupole broadening. On the contrary, the position of the diffuse magnetic region (high-field peak) distribution shifts toward higher fields up to ~350 kOe (at 77.4 K) and its partial contribution to the experimental spectrum progressively increases with the decrease of temperature. The above results show that the magnetic state in $CaMn_7O_{12}$ at $T<T_{M2}$ is intrinsically inhomogeneous, with paramagnetic contributions persisting down to temperatures much lower than the point of phase transition at T_{M2}. The complicated pattern of ^{57}Fe spectra indicates that this magnetic ordering is nonuniform, which perhaps appears owing to the formation of a microdomain structure or phase separation into magnetically ordered and paramagnetic phases.[18] For a more comprehensive analysis of the magnetic hyperfine structure of ^{57}Fe spectra, our Mössbauer experiments at lower temperatures ($T<T_{M1}$) are in progress.

CONCLUSIONS

Using Mössbauer spectroscopy, hyperfine interactions and structure of a local environment of ^{57}Fe probed atoms in the perovskite-like manganite $CaMn_7O_{12}$ are investigated. Magnetic measurements have shown that doping of the manganite structure by ^{57}Fe probe atoms does not affect its magnetic properties and values of the phase transition temperatures (T_{M1} and t_{M2}).

Mössbauer spectra at $T_{M2}\leq T\leq T_{CO}$ testify to the stabilization of a greater part of Fe^{3+} probe cations (>97%) in octahedral manganite $CaMn_7O_{12}$, replacing the manganese cations in $(Mn^{3+}O_6)$ [Fe(1) subspectrum] and $(Mn^{4+}O_6)$ [Fe(2) subspectrum] polyhedra. A very small part of Fe^{3+} probe cations characterized by very large quadrupole splitting has been attributed to the substitution for Mn^{3+} in $[Mn^{3+}(O_{(1)})_4]$ polyhedra with nearly square oxygen coordination or to the localization on the surface of the manganite particles.

The EFG calculations for the Mn^{3+} and Mn^{4+} positions show that the values of hyperfine parameters for Fe(1) and Fe(2) subspectra reflect a specificity of local structure of $(Mn^{3+}O_6)$ and $(Mn^{4+}O_6)$ polyhedra. Measurement of temperature dependence for the spectra at $T_{M2}\leq T\leq T_{CO}$ does not reveal any changes of oxidation state or local atomic environment for the ^{57}Fe probe atoms. In particular, any structural transitions in the vicinity of $T_C\approx 250$ K have not been detected, which in the literature was discussed in the frames of the charge modulation. Measurements in the cooling and heating modes did not reveal any hysteresis of the hyperfine parameters for the Fe(1) and Fe(2) quadrupole doublets.

It was shown that in the temperature interval 380 K$<T<$450 K, the ^{57}Fe Mössbauer spectra undergo a sharp change due to the nucleation of a cubic manganite phase and its gradual growth with an increase in temperature. At $T\geq 450$ K, the ^{57}Fe spectrum corresponds to single Fe^{3+} cation position in an oxygen symmetric octahedral surrounding.

At the temperature range $T<90$ K, an appearance of the magnetic partial subspectra with the hyperfine magnetic field values at ^{57}Fe nuclei up to ~350 kOe was observed. The given result is an independent experimental evidence of magnetic ordering in the manganese sublattice at $T\approx 90$ K.

ACKNOWLEDGMENTS

The authors would like to acknowledge financial support by the Russian Foundation for Basic Research–CNRS (Ref. No 05-03-22003), the French Research Agency CNRS (Department of Chemistry—PICS 3200), and the French Ministry for Foreign Affairs for supporting a Thesis in co-tutelle by University Bordeaux 1 "Sciences and Technology" and University Lomonosov Moscow (A.V.B.).

[1] M. Marezio, P. D. Dernier, J. Chenavas, and J. C. Joubert, J. Solid State Chem. **6**, 16 (1973).
[2] B. Bochu, J. Chenavas, J. C. Joubert, and M. Marezio, J. Solid State Chem. **11**, 88 (1974).
[3] J. Alonso, J. Sanchez-Benitez, H. Falcon, M. J. Martinez-Lope, and A. Munoz, Z. Naturforsch., B: Chem. Sci. **61**, 1507 (2006).
[4] R. Przenioslo, I. Sosnowska, E. Suard, A. Hewat, and A. N. Fitch, J. Phys.: Condens. Matter **14**, 5747 (2002).
[5] R. Przenioslo, W. van Beek, and I. Sosnowska, Solid State Commun. **126**, 485 (2003).

[6] I. O. Troyanchuk, L. S. Lobanovsky, N. V. Kasper, M. Hervieu, A. Maignan, C. Michel, H. Szymczak, and A. Szewczyk, Phys. Rev. B **58**, 14903 (1998).
[7] R. Przenioslo, I. Sosnowska, M. Zoltek, D. Hohlwein, and I. O. Troyanchuk, Physica B **241-243**, 730 (1998).
[8] R. Przenioslo, I. Sosnowska, D. Hohlwein, T. Hauss, and I. O. Troyanchuk, Solid State Commun. **111**, 687 (1999).
[9] R. Przenioslo, I. Sosnowska, P. Strunz, D. Hohlwein, T. Hauss, and I. O. Troyanchuk, Physica B **276-278**, 547 (2000).
[10] R. Przenioslo, I. Sosnowska, E. Suard, and T. Hansen, Appl. Phys. A: Mater. Sci. Process. **74**, S1731 (2002).
[11] R. Przenioslo, I. Sosnowska, E. Suard, A. Hewat, and A. N. Fitch, Physica B **344**, 358 (2004).
[12] I. O. Troyanchuk, L. A. Bashkirov, A. A. Shemyakov, and V. K. Prokopenko, Phys. Status Solidi A **89**, 601 (1985).
[13] I. O. Troyanchuk, A. Chernyi, and Y. G. Zonov, Sov. Phys. Solid State **31**, 283 (1989).
[14] E. A. Pomerantseva, D. M. Itkis, E. A. Goodilin, J. C. Noudem, M. V. Lobanov, M. Greenblatt, and Yu. D. Tretyakov, J. Mater. Chem. **14**, 1150 (2004).
[15] I. O. Troyanchuk, L. S. Lobanovsky, N. V. Kasper, M. Hervieu, A. Maignan, C. Michel, H. Szymczak, and A. Szewczyk, Phys. Rev. B **58**, 14903 (1998).
[16] Z. Zeng, M. Greenblatt, J. E. Sunstrom IV, and M. Croft, J. Solid State Chem. **147**, 185 (1999).
[17] O. Volkova, Yu. Arango, N. Tristan, V. Kataev, E. Goodilin, D. Meiyer, T. Lorentze, B. Bukhner, and A. Vasiliev, JETP Lett. **82**, 498 (2005).
[18] A. Prodi, G. Allodi, E. Gilioli, F. Licci, M. Marezio, F. Bolzoni, A. Gauzzi, and R. De Renzi, Physica B **374-375**, 55 (2006).
[19] V. Chechersky, A. Nath, I. Isaac, J. P. Franck, K. Ghosh, and R. I. Greene, J. Phys.: Condens. Matter **11**, 8921 (1999).
[20] A. Simopoulos, M. Pissas, G. Kallias, E. Devlin, N. Moutis, I. Panagiotopoulos, D. Niarchos, C. Christides, and R. Sonntag, Phys. Rev. B **59**, 1263 (1999).
[21] G. Kallias, M. Pissas, E. Devlin, and A. Simopoulos, Phys. Rev. B **65**, 144426 (2002).
[22] A. Tkachuk, K. Rogacki, D. E. Brown, B. Dabrowski, A. J. Fedro, C. W. Kimball, B. Pyles, X. Xiong, D. Rosenmann, and B. D. Dunlap, Phys. Rev. B **57**, 8509 (1998).
[23] A. Simopoulos, G. Kallias, E. Devlin, and M. Pissas, Phys. Rev. B **63**, 054403 (2000).
[24] A. M. Balagurov, V. Yu. Pomjakushin, D. V. Sheptyakov, V. L. Aksenov, N. A. Babushkina, L. M. Belova, O. Yu. Gorbenko, and A. R. Kaul, Eur. Phys. J. B **19**, 1434 (2004).
[25] V. S. Rusakov, Bull. Russ. Acad. Sci. Phys. **63**, 1093 (1999).
[26] I. A. Presniakov, A. V. Baranov, G. Demazeau, V. S. Rusakov, A. V. Sobolev, J. A. Alonso, M. J. Martinez-Lope, and K. Pokholok, J. Phys.: Condens. Matter **19**, 0362011 (2007).
[27] F. Menil, J. Phys. Chem. Solids **46**, 763 (1985).
[28] R. D. Shannon, Acta Crystallogr., Sect. A: Cryst. Phys., Diffr., Theor. Gen. Crystallogr. **32**, 751 (1976).
[29] B. Buffat, G. Demazeau, M. Pouchard, and P. Hagenmuller, Proc.-Indian Acad. Sci., Chem. Sci. **93**, 313 (1984).
[30] S. C. Bhargava, H. P. Kunkel, Sh. Singh, S. K. Malik, D. D. Buddhikot, and A. H. Morrish, Phys. Rev. B **71**, 104419 (2005).
[31] *Mössbauer Spectroscopy*, edited by D. P. E. Dickson and F. J. Berry (Cambridge University Press, Cambridge, 1986).
[32] R. M. Sternheimer, Phys. Rev. **130**, 1423 (1963).
[33] B. Bochu, J. L. Buevoz, J. Chenavas, A. Collomb, J. C. Joubert, and M. Marezio, Solid State Commun. **36**, 133 (1980).
[34] I. D. Brown, in *Stucture and Bonding in Crystals*, edited by M. O'Keefe and A. Navrotsky (Academic, New York, 1981).
[35] *Mössbauer Isomer Shift*, edited by G. K. Shenoy and F. E. Wagner (North-Holland, Amsterdam, 1978).
[36] Th. Sinnemann, R. Job, and M. Rosenberg, Phys. Rev. B **45**, 4941 (1992).
[37] C. W. Kimball, J. L. Matykiewicz, H. Lee, J. Giapintzakis, A. E. Dwight, B. D. Dunlap, J. D. Jorgensen, B. V. Weal, and F. A. Fradin, Physica C **156**, 547 (1988).
[38] W. Slawinski, R. Przenioslo, I. Sosnowska, M. Bieringer, I. Margiolaki, A. N. Fitch, and E. Suard, J. Solid State Chem. **179**, 2443 (2006).